Adhesion energy of single wall carbon nanotube loops on various substrates

Tianjun Li, Anthony Ayari, and Ludovic Bellon'

Adhesion energy of single wall carbon nanotube loops on various substrates

Tianjun Li,[1,2] Anthony Ayari,[3] and Ludovic Bellon[1,a]

[1]*Université de Lyon, Laboratoire de Physique, ENS de Lyon, CNRS-46, Allée d'Italie, Lyon 69364, France*
[2]*Department of Physics, Shaoxing University, 508 Huancheng West Rd., Shaoxing 312000, China*
[3]*Institut Lumière Matière, UMR5306 Université Lyon 1-CNRS, Université de Lyon, 69622 Villeurbanne Cedex, France*

The physics of adhesion of one-dimensional nano structures such as nanotubes, nano wires, and biopolymers on different substrates is of great interest for the study of biological adhesion and the development of nano electronics and nano mechanics. In this paper, we present force spectroscopy experiments of individual single wall carbon nanotube loops using a home-made interferometric atomic force microscope. Characteristic force plateaus during the peeling process allow the quantitative measurement of the adhesion energy per unit length on various substrates: graphite, mica, platinum, gold, and silicon. Moreover, using a time-frequency analysis of the deflection of the cantilever, we estimate the dynamic stiffness of the contact, providing more information on the nanotube configurations and its intrinsic mechanical properties. © *2015 Author(s). All article content, except where otherwise noted, is licensed under a Creative Commons Attribution 3.0 Unported License.* [http://dx.doi.org/10.1063/1.4919355]

I. INTRODUCTION

Since their discovery,[1] carbon nanotubes (CNTs) have attracted the interest of scientists for their unique electrical,[2] thermal,[3] and mechanical properties[4] and are foreseen as a major material in a huge range of applications in the next few decades, from materials reinforcement[5] to components of nanoscale electronics[6] and mechanics, for instance, nano-switches,[7] motors,[8] actuators,[9–11] etc. They are also widely used as a bench system to study fundamental physical phenomena on the mesoscopic scale and represent as such an archetype of nano-objects. Whatever exceptional their intrinsic properties are, their use in any application is linked to their interactions with their environment, mainly through the weak adhesive Van der Waals (VdW) force. The study of the VdW interaction between nanotubes and the rest of the world can thus help to understand the physics of polymer nanocomposites,[5,10,12] setae adhesion of geckos,[13] protein filament adhesion in mussels,[14] nanotube-tipped atomic force microscopy (AFM) probes,[15] nanoscale sensors,[16] gecko-foot-mimetic dry adhesives,[17] etc.

Up to now, the adhesive properties of nanotubes have been mostly probed by various smart but indirect measurements. Among those, Hertel and coworkers[18,19] imaged by AFM the shape of crossed nanotubes adsorbed on a silicon substrate. The profile of the top nanotube results from a balance of the deformation energy with the surface energy lost in this configuration, allowing the estimation of an adhesion energy when mechanical properties of the nanotubes are assumed. Kis and coworkers[20] performed a direct measurement using an AFM tip to pull the inner core of a telescopic multi wall CNT. Their experiment demonstrated a friction free interaction between the concentric layers and provides an estimation of the adhesion for this very specific geometry and material.

However, in these experiments, one usually accesses either intrinsic properties of the nanotube or its interaction with its environment using hypotheses on the other properties. Direct measurement of adhesive interactions can provide quantitative values of several properties in one single test and are thus an appealing method. For example, measurements of adhesion energy and Young's modulus of graphene layers on SiO_2 have been conducted in single bulge test experiments.[21] For nanotubes, a peeling test is a potentially powerful technique to characterize the adhesion properties of carbon nanotubes or nano wires with various substrates. A few experiments have been conducted,[22–27] along with theoretical/numerical modeling.[28,29] Quantitative measurements however have not been easily achieved, and the experimental data analysis relies on complex comparison with numerical simulations. We recently proposed a simpler protocol to perform peeling test,[30] which allow direct and quantitative characterization of the adhesion properties of nanotubes. A single wall CNT (SWCNT) is anchored to the tip of an AFM cantilever and is simply pushed almost perpendicularly to a flat surface. The VdW interaction causes part of the nanotube to adhere to the surface when the induced bending is strong enough, and the analysis of the force curve leads to quantitative information both on the adhesion process and on the nanotube itself.

In this paper, we present an extension of this protocol to CNT loops on various materials, leading to quantitative values of the energy of interaction of the nanotube with substrates of graphite, mica, platinum, gold, and silicon. We first present the samples (CNT and substrates) and the acquired data during approach-retract cycles: force, dynamic stiffness, and compression. We then give the analyzing framework

[a]ludovic.bellon@ens-lyon.fr

and discuss the nanotube configurations during peeling. We finally conclude, giving quantitative values of the adhesion energy of a SWCNT on the five different substrates.

II. EXPERIMENTS

A. Samples preparation

The nanotubes are grown directly[32] at the tip apex of AFM probes by Chemical Vapor Deposition (CVD): the bare silicon cantilevers are fully dipped into the catalyst solution, then gently dried in a nitrogen flux before being placed in the furnace. CNTs grow everywhere on the cantilever, and around 1 every 3 cantilevers present a CNT at the tip. The parameters are tuned to grow long SWCNT (a few micrometers), leading to a high probability of having nanotube loops (two anchoring points on the tip). A few Scanning Electron Microscopy (SEM) images of our samples right after the growth are presented in Figure 1. Note however that
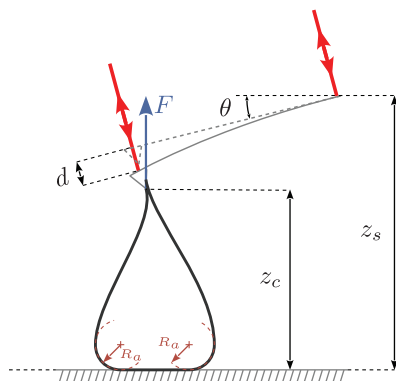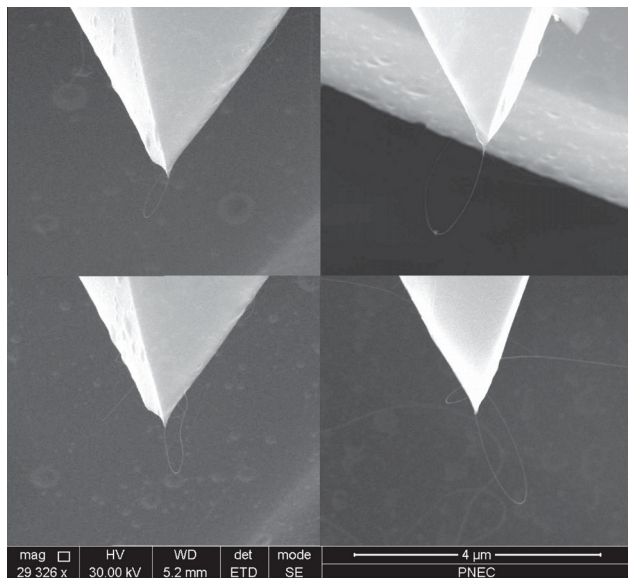

FIG. 1. (Top) Scanning electron micrographs of several SWCNTs grown directly on AFM tips. Long nanotubes tend to form loops on the tip, with a typical diameter around 1 μm. (Bottom) When the nanotube loop is pushed against a flat surface, part of the nanotube adheres to the surface due to Van der Waals interactions. The radius of curvature R_a at the last point of contact on the CNT with the substrate is fixed by an equilibrium between the adhesion of the part in contact and the bending of the free standing part of the nanotube. From the measurement of the AFM cantilever deflection d (using differential interferometry[31]) and sample position z_s, the force F acting on the nanotube and its compression z_c can be recorded.

nanotubes are often detected during AFM measurements, while they are not visible on the SEM images (the opposite is also true): the first contacts between the nanotube and the substrate have a strong influence on the nanotube shape. They can lift some CNTs from the tip, for example, or break their link to the tip. Only samples with reproducible behavior during numerous force cycles are considered in the present work.

For the substrates, we start with graphite and mica, since a fresh layer is always easy to be cleaved before the test. The three other substrates we choose to investigate the relative adhesion energies are surfaces of platinum (Pt), gold (Au), and silicon (Si). For the peeling tests, very flat surfaces are necessary in order to get rid of the impact from the morphology of the substrate. We choose to use chips of commercial AFM cantilevers as substrates, bare (thus Si surface) or with a coating of Pt or Au. Before the experiments, these 3 substrates undergo a cleaning process in an ultrasonic bath of ethanol for 10 min, isopropanol for 10 min, and then in a plasma cleaner (medium power) for 10 min to avoid any contamination from the environment. They are finally kept in a clean and dry container for 6 h to eliminate any potential surface impact of the cleaning process.

B. Force curves

In the experiments, the nanotube loop is pushed against a flat sample, as shown in the schematic diagram of Figure 1. The translation of the substrate is performed with a piezo translation platform (Physik Instrumente—PI P527.3) operated in closed loop, featuring an accuracy of 0.3 nm rms. We measure the deflection d of the AFM cantilever with a home-made highly sensitive quadrature phase differential interferometer, which detects the optical path difference between the sensing beam (focused on the cantilever tip) and the reference beam (focused on the static base—see sketch in Figure 1).[31,33,34] The deflection d and the sample vertical position z_s are simultaneously recorded with high resolution acquisition cards (National Instruments—NI-PXI-4462) at 200 kHz.

With both z_s and d being calibrated, using a proper definition of the origins, we can compute at any time the compression of the nanotube

$$z_c = z_s - d\cos\theta, \tag{1}$$

where $\theta = 15°$ accounts for the inclination of the cantilever with the substrate. We can also compute the vertical force acting on the nanotube

$$F = -\frac{k_s}{\cos\theta}d, \tag{2}$$

with k_s the static stiffness of the AFM cantilever (calibrated from its thermal noise[35]). Using compression instead of sample position allows us to take into account the compliance of the cantilever, thus to focus on the nanotube properties only in the force versus compression curves. An example of such a force curve is plotted in Figure 2 for a substrate of graphite. Several examples of force curves for different nanotubes are
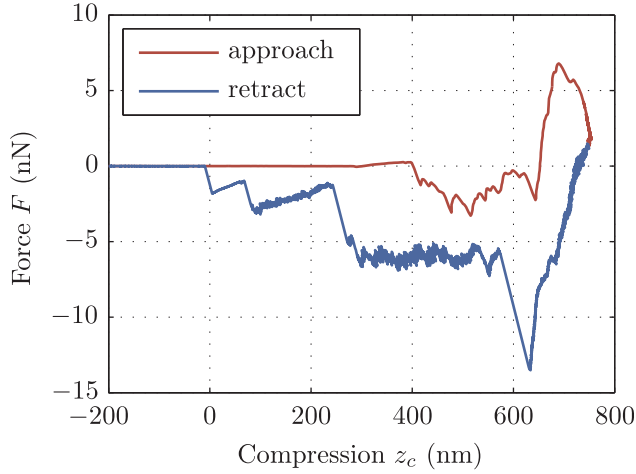
FIG. 2. Force F of a nanotube as a function of its compression z_c on a graphite substrate. A strong hysteresis, due to the adhesion, can be noticed between approach (red, top curve) and retraction (blue, bottom curve). Force plateaus, characteristic of a peeling mechanism, are observed during retraction.

also provided in the supplementary material.[36] A strong hysteresis can be noted during the approach-retract cycle, indicating that the nanotube is changing its configuration during compression. The force is mostly attractive (except at the end of the approach), hinting at adhesion as the main interaction process between the nanotube and the substrate. Most experiments are performed in air, but no difference in the force curves can be observed when experiments are performed in a dry atmosphere of nitrogen or in vacuum at 10^{-2} mbar: capillary forces are not involved in our experiments. Finally, we note long force plateaus during the retraction: this is the signature of a peeling process.[30]

Let us summarize the analysis presented in Ref. 30 to give grounds for this last claim. We denote by E_a the energy of adhesion per unit length of the nanotube on the surface. As soon as a small length of the nanotube is in contact with the substrate, the system tends to minimize its energy by maximizing the contact length. However, this process increases the bending of the free standing part of the nanotube and the associated curvature energy. The contact length is thus a balance between adhesion and bending, which leads to a constant radius of curvature R_a at the contact point. If the free standing part of the nanotube is long enough compared to R_a, its shape does not change much when it is being peeled from the surface. The vertical displacement δz needed to peel a small length δl from the surface is thus the same length: $\delta z \simeq \delta l$. In a quasi static displacement, the work produced by the pulling force $F\delta z$ is thus equivalent to the energy released $-2E_a\delta l$, leading to $F \simeq -2E_a$ (the factor 2 here accounts for the loop geometry of the CNT: we peel the same length δl for the two strands). Peeling a nanotube loop from a surface thus results in a flat force-compression curve, and the value of the force plateau gives directly the value of the adhesive energy per unit length. For the longest plateau of this nanotube on graphite, we read, for example, $E_a \simeq 3\,\mathrm{nJ/m}$.

For every CNT and substrate, we perform at least 50 approach-retract cycles: during the first contacts of the

nanotube, its configuration usually changes significantly before it reaches a stationary behavior. Some nanotubes can be lost during the process, others never reach a stable operation state. From the grown CNTs, we select only those having a clear peeling process signature: long force plateaus, similar force curves on various substrates, reproducible, and stable in time. Most indeed have many defects resulting in a too complex interpretation of the data (see first figure of supplementary material for an example[36]). For clarity, we present here the results corresponding to a single nanotube on various substrates. Its force signature is the clearest of our tests, and we observe similar behavior for other samples. No SEM image of this nanotube in its useful configuration is available. It is not visible in the SEM image performed right after the CNT growth. And as for all our nanotubes, it has eventually been lost after extensive force cycling on the various substrates, so no SEM image could be performed a posteriori. The force curves however are qualitatively similar to other CNT loops shown in the supplementary material.[36]

C. Dynamic stiffness

Following Refs. 30 and 37, during the approach-retract cycles, we also analyse the dynamic properties of the nanotube-substrate contact, by following the evolution of the thermal noise spectrum during the peeling process. Indeed, when the nanotube is in contact with the sample, the contact stiffness sums with the cantilever spring constant and leads to a higher resonance frequency of the system. The fluctuations of the deflection, driven by the random thermal noise excitation of the oscillator, allow us to track this frequency shift during contact, as illustrated in the inset of Figure 3: the power spectrum density (PSD) of the deflection S_d presents the characteristic Lorentzian shape of the thermal noise of a simple harmonic oscillator, peaked at frequencies ranging from 12 kHz (free cantilever, no contact) to 26 kHz (peeling configuration around $t = 5$ s).

From this frequency shift, one can recover the equivalent stiffness k_{CNT} of the CNT in contact with the substrate

$$k_{\mathrm{CNT}} = \frac{k_0}{\cos^2\theta}\left[\left(\frac{f_{\mathrm{CNT}}}{f_0}\right)^2 - 1\right], \qquad (3)$$

where f_0 and f_{CNT} are, respectively, the resonance frequency out of and in contact, and k_0 is the free cantilever dynamic stiffness. In this formula, we approximate the cantilever by a simple spring k_0, however when the frequency shift is significant as in this measurement, a complete Euler-Bernoulli description of the cantilever is better suited. It leads to the following relation between the dynamic contact stiffness and the resonance frequency of the first mode of the cantilever:[37]

$$k_{\mathrm{CNT}} = \frac{k_s}{\cos^2\theta}\frac{\alpha^3(1 + \cos\alpha\cosh\alpha)}{3(\cos\alpha\sinh\alpha - \sin\alpha\cosh\alpha)}, \qquad (4)$$

with

$$\alpha = \alpha_1\sqrt{\frac{f_{\mathrm{CNT}}}{f_0}}, \qquad (5)$$

FIG. 4. Dynamic stiffness k_{CNT} deduced from the resonance frequency f_{CNT} of the oscillator. When the dynamic stiffness is not too large compared to the static stiffness k_s of the free cantilever, a simple harmonic oscillator (SHO) model with a spring is sufficient. For larger values of k_{CNT}, a full Euler-Bernoulli model of the cantilever is required: a hard contact produces a finite frequency shift ($f_{CNT}/f_0 \approx 4.385$ when $k_{CNT} \to \infty$).

approximation is valid till $f_{CNT} \approx 2f_0$, but the full relation is better suited as soon as the contact stiffness is larger than the cantilever one.

To have a continuous information about the contact stiffness at any compression, we perform a time-frequency analysis of the deflection. We plot in Figures 3(a) and 3(b) the time trace of the sample position z_s and the deflection d, sampled at 200 kHz. We slice the latter signal in 5 ms time windows and compute in each window the PSD $S_d(t,f)$ of the deflection around the time t. Due to the short 5 ms time window, the frequency resolution is only 200 Hz, and the spectra are too noisy to be easily fitted. However, the maximum of the PSD $S_d(t,f)$ can be measured with the following estimator:

$$f_{CNT}(t) = \frac{\int_{\Delta f} f S_d(t,f)\,\mathrm{d}f}{\int_{\Delta f} S_d(t,f)\,\mathrm{d}f}, \qquad (6)$$

where Δf is an adequate frequency interval centered on f_{CNT} (self adapting procedure). The sampling rate for f_{CNT} is thus $1/5\,\mathrm{ms} = 200\,\mathrm{Hz}$. At such rate, one measures f_{CNT} every 0.6 nm of sample position during retraction. We plot the result of this procedure in Figure 3(c). From Eqs. (4) and (5), one finally computes the dynamic stiffness k_{CNT} of the nanotube in contact, and plot it in Figure 3(d). At the maximum compression of the nanotube, one sees from this analysis that we reach a hard contact between the AFM tip and the substrate: k_{CNT} reaches huge values (several N/m) compared to the cantilever stiffness ($k_s = (0.121 \pm 0.005)$ N/m) when $f_{CNT}/f_0 \approx 4.4$.
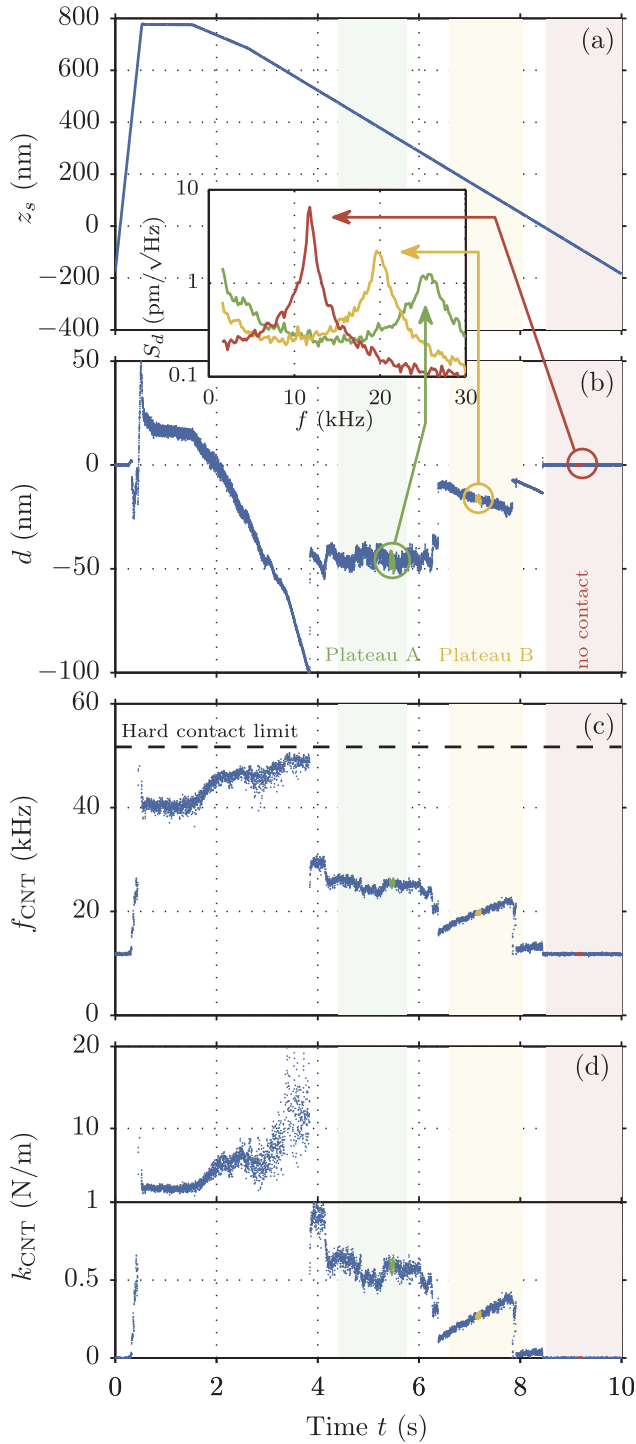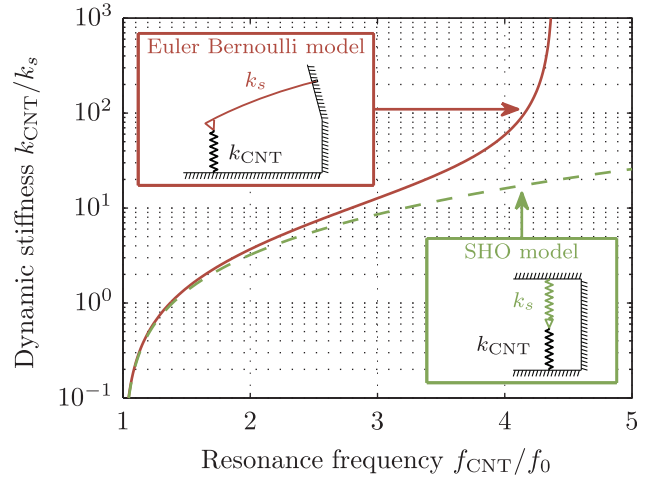

FIG. 3. Time evolution of: (a) the sample position z_s, (b) the deflection d, (c) the resonance frequency f_{CNT}, and (d) the dynamic stiffness k_{CNT} of the nanotube in contact during a slow approach-retract cycle (note the dual vertical scale of this last plot). The PSD S_d of the deflection, computed in a 0.1 s window around $t = 5$ s (green, peeling configuration, plateau A), $t = 7$ s (yellow, peeling configuration, plateau B), and $t = 9$ s (red, no contact), is shown in the inset. The shift of the resonance frequency of the oscillator (cantilever + nanotube in contact) can be used to compute the dynamic stiffness of the contact (see Figure 4). A time-frequency analysis allows one to track the maxima of the PSD computed in every 5 ms window, and then plot this frequency shift as a function of time in (c).

where $\alpha_1 \approx 1.875$ is the first spatial eigenvalue of a clamped-free Euler-Bernoulli mechanical beam. In Figure 4, we plot both relations 3 and 4: the simple spring

D. Mean interaction curves for the five substrates

For every substrate, we perform at least 10 very slow approach-retract cycles and compute for each the force $F(z_c)$

and dynamic stiffness $k_{CNT}(z_c)$ versus compression curves during the cycles. We then average these curves for each substrate and plot them in Figure 5. We focus here on the retractions only, which allow to probe the properties of the nanotube in a peeling configuration. The same nanotube is used for all the substrates.

The curves for the five different substrates have the same generic features: a steep force versus compression dependence and a huge dynamic stiffness at large compression, corresponding to a hard contact between the tip and the surface, then two distinct force plateaus (labelled A and B). The overall behavior is quite different in these two ranges of compression. For the first plateau (A), both F and k_{CNT} are rather flat. The average value of k_{CNT} increases with the adhesion force on the substrate. On plateau B, the force is also rather flat, but it almost does not depend on the sample (with the exception of graphite). The stiffness k_{CNT} presents a significant dependence on compression, with the highest values just before loosing contact, but is rather substrate independent. The shift between the 2 plateaus occurs at slightly different compressions for the five samples (the zero
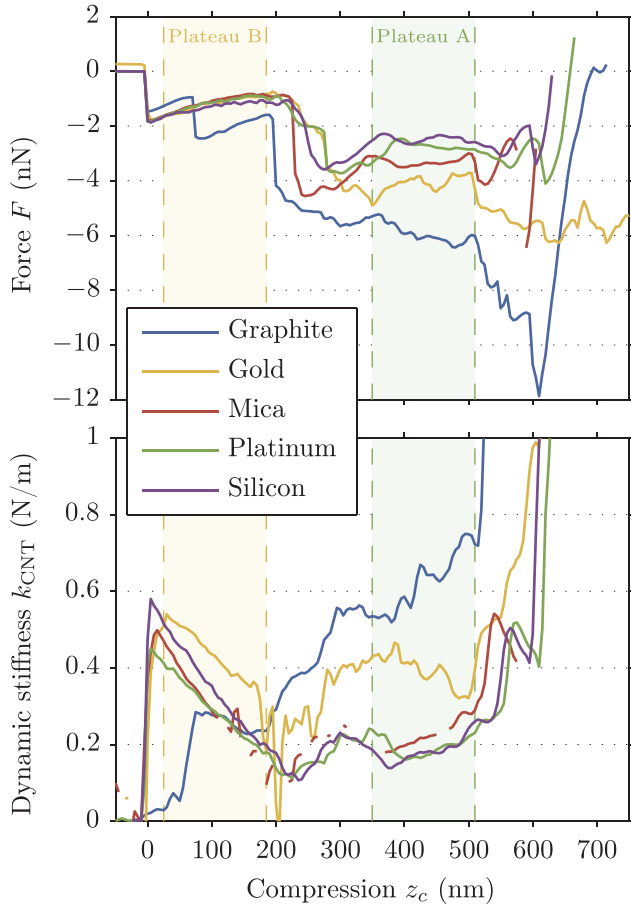

FIG. 5. Mean force F and dynamic stiffness k_{CNT} as a function of compression z_c measured during retraction on five different substrates: graphite, gold, mica, platinum, and silicon. Each curve is the average of a minimum of 10 approach-retract cycles. Two ranges of compression corresponding to force plateaus are defined: plateau A for $z_s = [350 - 510]$ nm and plateau B for $z_s = [35 - 185]$ nm. The zero of compression z_s is defined by the loss of contact between the nanotube and the substrate. Missing data in the dynamic stiffness curve for mica correspond to thermal noise spectra that are too noisy to extract the resonance frequency f_{CNT} and thus k_{CNT}.

of compression z_c is defined by the last contact point during retraction).

III. ADHESION ENERGY AND MECHANICAL PROPERTIES OF THE NANOTUBE

To understand the observed behavior, we use the framework of Ref. 30, corresponding to a straight nanotube initially almost perpendicular to the surface. In such case, a preliminary buckling is necessary to reach the adhered state. In the current work, we consider a nanotube loop that is inherently tangent to the surface before any contact. Adhesion processes are thus immediately relevant. The first contact leads directly to the adhesion of the nanotube. The loss of contact also starts directly with the CNT tangent to the surface, with no intermediate situation where only the tip of a straight nanotube is in contact. The behavior of the loop in contact is however equivalent to having two straight nanotubes sticking in parallel: the two free standing strands of the nanotube are independent since the part sticking to the substrate decouples them. The results of Ref. 30 are thus directly applicable, except that the measured force and contact stiffness should be divided by 2 for each strand of the nanotube!

Each part of the CNT in contact with the sample is thus described as an elastic line, incompressible along its axis. The shape of the line is given by a balance between adhesion and curvature, leading to the radius of curvature R_a at the last contact point before the free standing part

$$R_a = \sqrt{\frac{EI}{2E_a}}, \qquad (7)$$

where E_a is the energy of adhesion per unit length, E the nanotube Young's modulus, and $I = \pi d_{CNT}^3 t_{CNT}/8$ its quadratic moment (d_{CNT} its diameter, t_{CNT} the wall thickness—0.34 nm for a SWCNT[11]). As long as the free standing part of the nanotube is much larger than R_a, if we neglect horizontal components of the interaction, the force of interaction with the substrate should be constant and equal to $-E_a$,[30] hence

$$F = -2E_a, \qquad (8)$$

for a CNT loop.

The static stiffness, defined as dF/dz_c is thus zero on the force plateau. However, as clearly illustrated in Figure 3 or 5, the dynamic stiffness measured at the resonance frequency of the oscillator (cantilever + CNT in contact) is not zero: at a few tens of kHz, adhesion has no time to be switched on and off by the small thermal fluctuations, and the sticking part of the CNT can be considered as rigidly clamped to the substrate. In such a case, using the same hypotheses (long nanotube, negligible horizontal forces, and 2 strands), we compute for the dynamic stiffness[30]

$$k_{CNT} = 2\left(1 + \sqrt{2}\right)\frac{E_a}{R_a} = 8\left(1 + \sqrt{2}\right)\sqrt{\frac{E_a^3}{\pi E d_{CNT}^3 t_{CNT}}}. \qquad (9)$$

The dynamic stiffness should therefore present a plateau in correspondence to the force one, with values scaling as $E_a^{3/2}$.

In this analysis framework, we suppose for simplicity that the quadratic moment I of the nanotube is that of an ideal SWCNT. Our samples may differ from this model, as they may be made of bundles of a few single wall nanotubes, carry a significant amount of amorphous carbon,[38] or be few-wall nanotubes. The inferred diameter d_{CNT} should therefore be considered carefully, but nevertheless provides a reasonable order of magnitude for the probed nanotube.

To test those ideas, we compute for the five substrates the joint histograms of k_{CNT} and F during all the retractions and plot them in Figure 6. As clearly illustrated in this figure, the CNT adopts two different configurations during peeling, corresponding to plateaus A and B. We also report in the bottom plot of Figure 6 the mean values of k_{CNT} and F on the 2 plateaus defined in Figure 5 for each substrate. The data for plateau A are consistent with our model of peeling a CNT in the direction normal to the surface: constant force F, constant dynamic stiffness k_{CNT}, both depending on the substrate material, but all sharing the same nanotube diameter $d_{CNT} \approx 3$ nm.

The behavior on plateau B is not well described by the model: except for graphite which presents 2 different configurations during this range of compression, both F and k_{CNT} depend on compression but not on the substrate. This can be the signature of an adhesion process of the nanotube loop on the silicon tip. Indeed, the two nanotube strands are not perfectly at the tip apex (or the hard contact we reach during the cycle would certainly break their clamping), so they can present some adhesion/peeling mechanism. In such case, the signature should be quite independent of the substrate on the other side of the nanotube. Moreover, the peeling of the nanotube from the AFM tip is not normal to the surface of the silicon tip, so our model may not be suited: the force component parallel to the surface is not negligible any more, so the force and dynamic stiffness can depend on compression. The case of the graphite substrate, implying larger forces, apparently leads to different nanotube configurations in the range of compression corresponding to plateau B.

We finally focus of the range of compression corresponding to plateau A only. The observations of the force and dynamic stiffness plateaus are well described by a peeling configuration, corresponding to a nanotube loop with $d_{CNT} = 3$ nm. The corresponding values of the adhesion energies of the five substrates are reported in Table I: graphite has the strongest interaction with the CNT at (2.96 ± 0.33) nJ/m, while silicon has the lowest at (1.24 ± 0.11) nJ/m. Those numbers are in the same order of magnitude as others reported in the literature,[18–24,39–42] though we notice a factor of 3 with our previous measurements on graphite and mica.[30] However, the nanotubes of those 2 sets of experiments were grown at a different time in different laboratories and may have some different adhesion properties due to different chiralities, amount of amorphous carbon around the SWCNT,[38] number of bundled SWCNT, etc. The ratio between the energy of adhesion is anyway preserved (nanotubes stick twice more on graphite than on mica), so the relative values of the substrates presented in Table I are of broad utility.
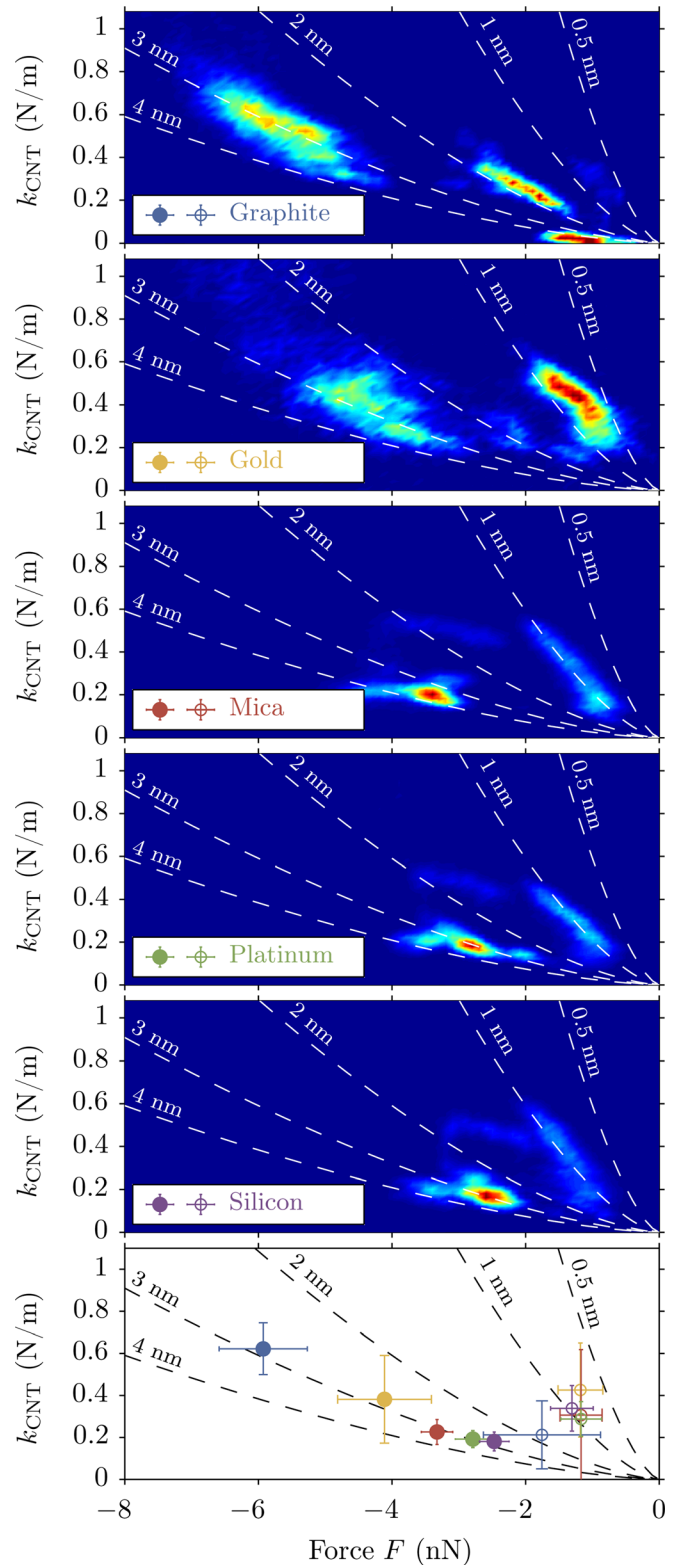

FIG. 6. To understand the configurations of the CNT during retraction, we plot the joint histograms of k_{CNT} and F, for the five substrates. The relation expected between k_{CNT} and F for adhered SWCNT loops of various diameters $d_{CNT} = [0.5, 1, 2, 3, 4]$ nm is superposed on the graphs. The nanotube explores mainly 2 different configurations: one at low force-low stiffness (plateau B) and one at higher force and stiffness (plateau A). The mean value and standard deviation of k_{CNT} and F on the two plateaus are plotted in the bottom graph (plain circles for A, empty circles for B). The configuration of plateau A agrees well with the model, with an estimated diameter $d_{CNT} \approx 3$ nm for all the substrates. The configuration of plateau B would correspond to $d_{CNT} \approx 1$ nm, but show no substrate dependence and is attributed to adhesion on the AFM tip.

TABLE I. Adhesion energies of a SWCNT on various substrates. The values of E_a may differ for different nanotube parameters (diameter, chirality, purity, and additional amorphous carbon layer), but not their relative values. The uncertainty corresponds to the standard deviation in the range of compression corresponding to plateau A for all forces curves on each substrate.

Substrate	E_a (nJ/m)
Graphite	2.96 ± 0.33
Gold	2.06 ± 0.35
Mica	1.66 ± 0.12
Platinum	1.39 ± 0.13
Silicon	1.24 ± 0.11

IV. CONCLUSION

In this article, we present some experiments where a SWCNT loop, grown directly on an AFM tip, is pushed against various substrates. The adhesion force and dynamic stiffness of the nanotube in contact with the sample are recorded as a function of its compression. The experimental data are analyzed in the framework of an elastic loop sticking to a flat surface. During retraction, we observe force plateaus characteristic of a mechanism of peeling. The cross-information between force and dynamic stiffness helps to understand the configuration of the nanotube during the peeling process: some of the plateaus are attributed to adhesion on the substrate, while others are hinting at adhesion on the AFM tip. Quantitative values are derived for the diameter of the nanotube and its energy of adhesion per unit length on various substrates: graphite, gold, mica, platinum, and silicon.

Our experiments illustrate how CNT loops are useful nano-objects to probe peeling processes at the nanoscale, leading to a quantitative measurement of their Van der Walls interaction with flat substrates. This work provides an interesting insight into the physical mechanism of adhesion and should be helpful in the design of nanotube-based nanomechanical devices: if adhesion is sought (for clamping purposes for example), graphite is a good candidate, whereas low interaction can be obtained using a silicon substrate. Other materials of technological relevance could be characterized using our simple protocol.

[1]S. Iijima, Nature **363**, 603 (1993).
[2]Z. Yao, C. L. Kane, and C. Dekker, Phys. Rev. Lett. **84**, 2941 (2000).
[3]S. Iijima, Nature **354**, 56 (1991).
[4]G. Lanzani and L. Luer, in *Comprehensive Nanoscience and Technology*, edited by D. L. Andrews, G. D. Scholes, and G. P. Wiederrecht (Academic Press, Amsterdam, 2011), pp. 23–39.
[5]S. Bal and S. Samal, Bull. Mater. Sci. **30**, 379 (2007).
[6]P. G. Collins and P. Avouris, Sci. Am. **283**, 62 (2000).
[7]J. Cumings and A. Zettl, Science **289**, 602 (2000).
[8]A. M. Fennimore, T. D. Yuzvinsky, W.-Q. Han, M. S. Fuhrer, J. Cummings, and A. Zettl, Nature **424**, 408 (2003).
[9]C. Ke and H. D. Espinosa, Appl. Phys. Lett. **85**, 681 (2004).
[10]O. Breuer and U. Sundararaj, Polym. Compos. **25**, 630 (2004).
[11]A. Kis and A. Zettl, Philos. Trans. R. Soc., A **366**, 1591 (2008).
[12]F. Hussain, M. Hojjati, M. Okamoto, and R. E. Gorga, J. Compos. Mater. **40**, 1511 (2006).
[13]M. A. Correa-Duarte, N. Wagner, J. Rojas-Chapana, C. Morsczeck, M. Thie, and M. Giersig, Nano Lett. **4**, 2233 (2004).
[14]M. J. Sever, J. T. Weisser, J. Monahan, S. Srinivasan, and J. J. Wilker, Angew. Chem., Int. Ed. **43**, 448 (2004).
[15]M. C. Strus, A. Raman, C.-S. Han, and C. V. Nguyen, Nanotechnology **16**, 2482 (2005).
[16]B. Mahar, C. Laslau, R. Yip, and Y. Sun, IEEE Sens. J. **7**, 266 (2007).
[17]L. Qu, L. Dai, M. Stone, Z. Xia, and Z. L. Wang, Science **322**, 238 (2008).
[18]T. Hertel, R. Martel, and P. Avouris, J. Phys. Chem. B **102**, 910 (1998).
[19]T. Hertel, R. E. Walkup, and P. Avouris, Phys. Rev. B **58**, 13870 (1998).
[20]A. Kis, K. Jensen, S. Aloni, W. Mickelson, and A. Zettl, Phys. Rev. Lett. **97**, 025501 (2006).
[21]S. P. Koenig, N. G. Boddeti, M. L. Dunn, and J. S. Bunch, Nat. Nanotechnol. **6**, 543 (2011).
[22]M. Ishikawa, R. Harada, N. Sasaki, and K. Miura, Appl. Phys. Lett. **93**, 083122 (2008).
[23]M. Ishikawa, R. Harada, N. Sasaki, and K. Miura, Phys. Rev. B **80**, 193406 (2009).
[24]C. Ke, M. Zheng, G. Zhou, W. Cui, N. Pugno, and R. N. Miles, Small **6**, 438 (2010).
[25]M. C. Strus, R. R. Lahiji, P. Ares, V. Lopez, A. Raman, and R. Reifenberger, Nanotechnology **20**, 385709 (2009).
[26]H. Xie and S. Regnier, Rev. Sci. Instrum. **81**, 035112 (2010).
[27]K. M. Barker, M. A. Poggi, L. Lizarraga, P. T. Lillehei, A. A. Ferri, and L. A. Bottomley, J. Nanotechnol. **2014**, 349453 (2014).
[28]X. Oyharcabal and T. Frisch, Phys. Rev. E **71**, 036611 (2005).
[29]N. Sasaki, A. Toyoda, N. Itamura, and K. Miura, J. Surf. Sci. Nanotechnol. **6**, 72 (2008).
[30]J. Buchoux, L. Bellon, S. Marsaudon, and J.-P. Aimé, Eur. J. Phys. B **84**, 69 (2011).
[31]P. Paolino, F. A. Sandoval, and L. Bellon, Rev. Sci. Instrum. **84**, 095001 (2013).
[32]L. Marty, A. Iaia, M. Faucher, V. Bouchiat, C. Naud, M. Chaumont, T. Fournier, and A. Bonnot, Thin Solid Films **501**, 299 (2006).
[33]C. Schonenberger and S. F. Alvarado, Rev. Sci. Instrum. **60**, 3131 (1989).
[34]L. Bellon, S. Ciliberto, H. Boubaker, and L. Guyon, Opt. Commun. **207**, 49 (2002).
[35]H. J. Butt and M. Jaschke, Nanotechnology **6**, 1 (1995).
[36]See supplementary material at http://dx.doi.org/10.1063/1.4919355 for SEM images of various CNT tips and associated forces curves on a graphite substrate.
[37]J. Buchoux, J.-P. Aimé, R. Boisgard, C. V. Nguyen, L. Buchaillot, and S. Marsaudon, Nanotechnology **20**, 475701 (2009).
[38]Z. An, A. Furmanchuk, R. Ramachandramoorthy, T. Filleter, M. R. Roenbeck, H. D. Espinosa, G. C. Schatz, and S. T. Nguyen, Carbon **80**, 1 (2014).
[39]L. A. Girifalco, M. Hodak, and R. S. Lee, Phys. Rev. B **62**, 13104 (2000).
[40]B. Chen, M. Gao, J. Zuo, S. Qu, B. Liu, and Y. Huang, Appl. Phys. Lett. **83**, 3570 (2003).
[41]M. C. Strus, L. Zalamea, A. Raman, R. B. Pipes, C. V. Nguyen, and E. A. Stach, Nano Lett. **8**, 544 (2008).
[42]M. C. Strus, C. I. Cano, R. B. Pipes, C. V. Nguyen, and A. Raman, Compos. Sci. Technol. **69**, 1580 (2009).